






RESEARCH ARTICLE | NOVEMBER 05 2024

## Interatomic Coulombic electron capture beyond the virtual photon approximation

Jan Šenk ; Vincent Graves ; Jimena D. Gorfinkiel ; Přemysl Koloreň ; Nicolas Sisourat  



*J. Chem. Phys.* 161, 174113 (2024)

<https://doi.org/10.1063/5.0227540>



### Articles You May Be Interested In

Transforming underground to surface mining operation – A geotechnical perspective from case study

*AIP Conference Proceedings* (November 2021)

Monthly prediction of rainfall in nickel mine area with artificial neural network

*AIP Conference Proceedings* (November 2021)

Estimation of Karts groundwater based on geophysical methods in the Monggol Village, Saptosari District, Gunungkidul Regency

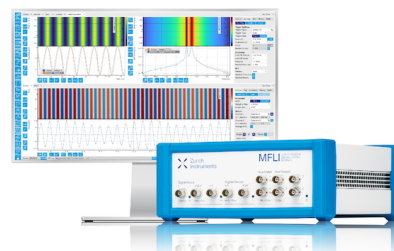
*AIP Conference Proceedings* (November 2021)

## Challenge us.

What are your needs for periodic signal detection?



[Find out more](#)



# Interatomic Coulombic electron capture beyond the virtual photon approximation

Cite as: J. Chem. Phys. 161, 174113 (2024); doi: 10.1063/5.0227540

Submitted: 9 July 2024 • Accepted: 16 October 2024 •

Published Online: 5 November 2024



View Online



Export Citation



CrossMark

Jan Šenk,<sup>1,2,a)</sup> Vincent Graves,<sup>3</sup> Jimena D. Gorfinkiel,<sup>3</sup> Přemysl Koloreňč,<sup>2</sup> and Nicolas Sisourat<sup>1,b)</sup>

## AFFILIATIONS

<sup>1</sup>Sorbonne Université, CNRS, Laboratoire de Chimie Physique Matière et Rayonnement, UMR 7614, F-75005 Paris, France

<sup>2</sup>Institute of Theoretical Physics, Faculty of Mathematics and Physics, Charles University, V Holešovičkách 2, 180 00 Prague, Czech Republic

<sup>3</sup>School of Physical Sciences, The Open University, Walton Hall, Milton Keynes MK7 6AA, United Kingdom

<sup>a)</sup>jan.senk@sorbonne-universite.fr

<sup>b)</sup>Author to whom correspondence should be addressed: Nicolas.Sisourat@sorbonne-universite.fr

## ABSTRACT

Via the interatomic Coulombic electron capture (ICEC) process, an electron can be captured by an atom or a molecule, while the binding and excess energy is transferred, via a long-range Coulomb interaction, to a neighboring atom or molecule. The transferred energy can be used to ionize or electronically excite the neighboring species. When the two species are asymptotically far apart, an analytical formula for the ICEC cross sections can be derived. The latter can then be estimated using only the energies and the photoionization cross sections of each species. In this work, we develop an analytical model that allows us to predict the ICEC cross sections when the size of the involved species is comparable to the distance between the two entities. Using *ab initio* R-matrix results for various systems, we show that the new model reduces the error of the asymptotic formula by two orders of magnitude on average while only using parameters that can be taken from the properties of each species.

Published under an exclusive license by AIP Publishing. <https://doi.org/10.1063/5.0227540>

## I. INTRODUCTION

In interatomic Coulombic electron capture (ICEC), an electron is captured by one neutral or positively charged atom or molecule while the binding and excess energy is transferred, via a long-range Coulomb interaction, to a neighboring atom or molecule. The latter can be ionized or electronically excited. ICEC was discovered and first investigated using analytical scattering theory.<sup>1,2</sup> Later on, *ab initio* calculations using the R-matrix method were performed.<sup>3,4</sup> A recent review on ICEC can be found in Ref. 5.

Using the dipole–dipole coupling approximation, also called the virtual photon approximation (VPA), an analytical formula for the ICEC cross sections can be derived.<sup>1,2</sup> The cross sections can be estimated using only the energies and the photoionization cross sections of each species. However, the approximation assumes that the two species are asymptotically far apart and therefore is inadequate when the size of the involved species is comparable to the distance between the two entities. *Ab initio* R-matrix calculations showed that in this close interatomic distance range, the ICEC cross sections are a

few orders of magnitude larger.<sup>3,4</sup> Despite this limitation, having an analytical formula for the ICEC cross sections that relies only on the tabulated data of each species allows for a simple and fast estimate of the ICEC efficiency.

In this study, we develop an analytical model that allows us to predict the ICEC cross sections beyond the VPA while keeping a simple description of the whole system as two independent entities. Furthermore, we show that the parameters of our novel formula can be taken from the properties of each species as in the VPA. In comparison with first-principles ICEC cross sections, our model reduces the error by about two orders of magnitude on average with respect to the virtual photon approximation at interatomic distances comparable to the size of the involved species.

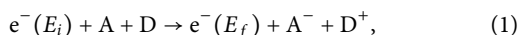
This paper is organized as follows: In Sec. II, we define the model and derive the formula for the ICEC cross sections within that model. This is followed by a brief summary of the R-matrix method and the computational details in Sec. III. In Sec. IV, we evaluate the parameters of the model by fitting it to *ab initio* cross sections for several systems. Then, we compare the *ab initio* cross sections with

the approximation by the VPA and by our model in the systems that have been used for the fitting, as well as systems that have not been considered in the fitting stage. The latter represent a test for our new model. Hartree atomic units are used throughout this paper unless explicitly mentioned otherwise.

## II. ANALYTICAL MODEL BEYOND THE VIRTUAL PHOTON APPROXIMATION

In the following, we derive an approximate formula that takes into account the overlap of acceptor and donor orbitals. We use the formalism of nonrelativistic quantum scattering theory from Ref. 6. We confine ourselves to the fixed-nuclei approximation and investigate the electronic problem only.

Consider the ICEC process



where  $E_i$  (and  $E_f$ ) are the energies of the incoming (and outgoing) electron, A stands for the acceptor of the electron, and D is the donor of the ICEC electron. Both the acceptor and the donor can be atoms, molecules, or ions. In all the processes considered in this paper, the donor is a neutral species and the acceptor is a singly ionized cation (i.e.,  $A^-$  is a neutral species). The differential cross section is given by

$$\frac{d\sigma}{d\Omega}(\mathbf{k}_f, A^-D^+ \leftarrow \mathbf{k}_i, AD) = \frac{k_f}{k_i} \left| \hat{f}(\mathbf{k}_f, A^-D^+ \leftarrow \mathbf{k}_i, AD) \right|^2, \quad (2)$$

where  $\mathbf{k}_i$  (and  $\mathbf{k}_f$ ) is the wave vector of the incoming (and outgoing) electron and  $\hat{f}$  is the scattering amplitude of the process.

From the scattering theory perspective, ICEC is a multichannel inelastic process where an electron is scattered on a target containing  $N$  bound electrons. For such a general process, the system's electronic wave function is antisymmetrized to satisfy the Pauli exclusion principle. The antisymmetrization gives rise to two contributions to the scattering amplitude,<sup>6</sup>

$$\hat{f}(\mathbf{k}_f, A^-D^+ \leftarrow \mathbf{k}_i, AD) = f_{\text{di}}(\mathbf{k}_f, A^-D^+ \leftarrow \mathbf{k}_i, AD) - N f_{\text{ex}}(\mathbf{k}_f, A^-D^+ \leftarrow \mathbf{k}_i, AD). \quad (3)$$

On the right-hand side, the scattering electron is already treated as distinguishable from the  $N$  target electrons. The *direct* contribution  $f_{\text{di}}$  assumes that the outgoing electron and the incoming electron are the same one, and the process is an inelastic scattering of this electron, which causes a rearrangement of the target. In ICEC, we call this the *electron transfer* contribution. The *exchange* contribution  $f_{\text{ex}}$  is the complementary process. More specifically, for ICEC, the acceptor subsystem of the target captures the incoming electron, and the excess energy is released by the donor subsystem, emitting the outgoing electron. We call this the *virtual photon* contribution.

The lowest order approximation of the exchange term leads to the VPA. The detailed derivation was given in Refs. 1 and 2. We also mention that a similar formula was derived using molecular quantum electrodynamics theory for the case of resonant energy transfer (see, for example, Refs. 7 and 8.) Let us summarize the main steps as follows.<sup>1</sup> Denoting  $R$  the distance between the centers of mass of A and D, we assume that  $R$  is much larger than the size of A and

D. This eliminates the overlap of the two subsystems. We use the distorted-wave Born approximation (DWBA).<sup>6</sup> The initial state is the electron incoming into subsystem A (not interacting with D), and the final state is the electron outgoing from  $D^+$  (not interacting with  $A^-$ ). The two subsystems interact with each other via the Coulomb interaction of two groups of electrons separated by the distance  $R$ . Then, we use the multipole expansion and notice that the lowest non-vanishing term corresponds to the dipole-dipole interaction of the two charge densities and is proportional to  $R^{-3}$ . The integral of the differential cross section over the scattering angle gives the total cross section. We use the definition of the photoionization and photorecombination cross sections and apply the principle of detailed balance to convert the photorecombination cross sections into photoionization cross sections. The final result is (in SI units)<sup>2</sup>

$$\sigma_{\text{VPA}} = \frac{3\hbar^4 c^2}{8\pi m_e} \frac{g_{A^-} \sigma_{\text{PI}}^{(A^-)}(E_i) \sigma_{\text{PI}}^{(D)}(E_f)}{g_A E_i R^6 E_{\text{vph}}^2}, \quad (4)$$

where  $g_A$  and  $g_{A^-}$  are the multiplicities of the corresponding states,  $\sigma_{\text{PI}}$  are the photoionization cross sections, and  $E_{\text{vph}}$  is the energy of the virtual photon given by

$$E_{\text{vph}} = E_i + EA_A = E_f + IP_D, \quad (5)$$

where EA is the electron affinity and IP is the ionization energy.

We continue with the direct contribution. As for the exchange contribution, we consider only the lowest order term. High-order corrections are expected to be much smaller. The in-channel of the direct contribution is an incoming electron scattering off of AD. The out-channel is an outgoing electron scattering off of  $A^-D^+$ ,

$$|\Psi_{\text{in}}\rangle = |\mathbf{k}_i+\rangle |\Psi_{AD}\rangle, \quad (6)$$

$$|\Psi_{\text{out}}\rangle = |\mathbf{k}_f-\rangle |\Psi_{A^-D^+}\rangle. \quad (7)$$

We divide the scattering potential in both channels into two parts,

$$V_{\text{I}}^{\text{in}} = - \sum_{\alpha \in AD} \frac{Z_\alpha}{|\mathbf{r} - \mathbf{R}_\alpha|} + \sum_{i \in AD} \frac{1}{|\mathbf{r} - \mathbf{r}_i|}, \quad (8)$$

$$V_{\text{II}}^{\text{in}} = \sum_{i \in A} \sum_{j \in D} \frac{1}{|\mathbf{r}_i - \mathbf{r}_j|}, \quad (9)$$

$$V_{\text{I}}^{\text{out}} = - \sum_{\alpha \in A^-D^+} \frac{Z_\alpha}{|\mathbf{r} - \mathbf{R}_\alpha|} + \sum_{i \in A^-D^+} \frac{1}{|\mathbf{r} - \mathbf{r}_i|}, \quad (10)$$

$$V_{\text{II}}^{\text{out}} = \sum_{i \in A^-} \sum_{j \in D^+} \frac{1}{|\mathbf{r}_i - \mathbf{r}_j|}. \quad (11)$$

The positions of the nuclei are denoted by  $\mathbf{R}_\alpha$ , and their charges are denoted by  $Z_\alpha$ . The position of the continuum electron is denoted by  $\mathbf{r}$ , and the positions of the target electrons are denoted by  $\mathbf{r}_i$  and  $\mathbf{r}_j$ . The potentials with the subscript I are chosen so that they cannot cause the process we are seeking—transfer of an electron from D to A. They are describing the interaction of the continuum electron with the target system. The potentials with the subscript II describe

the interaction of the electrons of the two subsystems, A and D in the in-channel and  $A^-$  and  $D^+$  in the out-channel.

We may now use the DWBA to obtain the approximation of the desired scattering amplitude,<sup>6</sup>

$$f_{\text{di}}(\mathbf{k}_f, A^-D^+ \leftarrow \mathbf{k}_i, AD) \approx -(2\pi)^2 \langle \Psi_{\text{out}} | V_{\text{II}}^{\text{out}} | \Psi_{\text{in}} \rangle. \quad (12)$$

In  $V_{\text{II}}^{\text{out}}$ , it is assumed that the electrons of  $A^-$  are separated from the electrons of  $D^+$ , with the distance being  $R$ . We may employ the multipole expansion [see Fig. 4 and Eq. (52) of Ref. 9], which in the lowest order gives

$$f_{\text{di}}(\mathbf{k}_f, A^-D^+ \leftarrow \mathbf{k}_i, AD) \approx -(2\pi)^2 \frac{\langle \mathbf{k}_f - |\mathbf{k}_i+\rangle | \Psi_{A^-D^+} | \Psi_{AD} \rangle}{R}. \quad (13)$$

This contribution is nontrivial because we do not assume that the two overlaps in the numerator are zero.

Now, we formulate a simplified model that we use to obtain an expression for the cross sections of the electron transfer contribution to ICEC. First, we focus on the overlap of the target states  $S_{AD} = \langle \Psi_{A^-D^+} | \Psi_{AD} \rangle$ . In a Hartree-Fock-like picture, the two states comprise the following occupied spin-orbitals:

$$|\Psi_{AD}\rangle = |\psi_1^A \dots \psi_{n_A}^A \psi_1^D \dots \psi_{n_D}^D\rangle, \quad (14)$$

$$|\Psi_{A^-D^+}\rangle = |\psi_1^A \dots \psi_{n_A+1}^A \psi_1^D \dots \psi_{n_D-1}^D\rangle, \quad (15)$$

where  $n_A + n_D = N$ . The overlap becomes

$$S_{AD} = \langle \psi_{n_A+1}^A | \psi_{n_D}^D \rangle. \quad (16)$$

For the sake of simplicity of the model, we assume that the two corresponding spin-orbitals have the same spin and they are Gaussians with widths  $a_A$  and  $a_D$ , whose centers are at mutual distance  $R$ ,

$$\langle \mathbf{r} | \psi_{n_A+1}^A \rangle = (\pi a_A^2)^{-3/4} \exp\left(-\frac{(\mathbf{r} - \mathbf{R}/2)^2}{2a_A^2}\right), \quad (17)$$

$$\langle \mathbf{r} | \psi_{n_D}^D \rangle = (\pi a_D^2)^{-3/4} \exp\left(-\frac{(\mathbf{r} + \mathbf{R}/2)^2}{2a_D^2}\right). \quad (18)$$

The overlap then amounts to

$$S_{AD} = \left(\frac{2a_A a_D}{a_A^2 + a_D^2}\right)^{3/2} \exp\left(-\frac{R^2}{2(a_A^2 + a_D^2)}\right). \quad (19)$$

The continuum electrons  $|\mathbf{k}_i+\rangle$  and  $|\mathbf{k}_f-\rangle$  are the solutions of the time-independent Schrödinger equation with appropriate boundary conditions with the potential generated from  $|\Psi_{AD}\rangle$  and  $|\Psi_{A^-D^+}\rangle$ , respectively. We take into account only the spherical contributions to these potentials, which allows us to use the partial wave expansion and obtain<sup>6</sup>

$$\langle \mathbf{r} | \mathbf{k}_{i/f} \rangle = \frac{1}{\sqrt{2\pi^3}} \frac{1}{r} \sum_{l=0}^{\infty} (2l+1) i^l \psi_{l, \mathbf{k}_{i/f}}^{\pm}(r) P_l(\hat{\mathbf{r}} \cdot \hat{\mathbf{k}}_{i/f}), \quad (20)$$

where the hat denotes unit vectors,  $\psi_{l, \mathbf{k}_{i/f}}^{\pm}$  are the radial incoming/outgoing scattering wave functions, and  $P_l$  is the Legendre polynomial. Evaluating the overlap yields

$$\langle \mathbf{k}_f - |\mathbf{k}_i+\rangle = \frac{1}{2\pi^2 k_i k_f} \int_0^{\infty} dr \sum_{l=0}^{\infty} (2l+1) \psi_{l, \mathbf{k}_f}^{-*}(r) \psi_{l, \mathbf{k}_i}^{+}(r) P_l(\hat{\mathbf{k}}_i \cdot \hat{\mathbf{k}}_f). \quad (21)$$

Now, let us gather the results for the differential cross section of the lowest order contribution to the electron transfer path of ICEC within our model by substituting (13) and (19) into (2),

$$\frac{d\sigma}{d\Omega} = \frac{k_f}{k_i} (2\pi)^4 \frac{1}{R^2} S_{AD}^2 |\langle \mathbf{k}_f - |\mathbf{k}_i+\rangle|^2. \quad (22)$$

Our goal is to obtain the corresponding total cross section,

$$\sigma = \int d\Omega \frac{d\sigma}{d\Omega}. \quad (23)$$

The only angle-dependent part of the differential cross section formula is the overlap of the continuum electrons,

$$\int d\Omega |\langle \mathbf{k}_f - |\mathbf{k}_i+\rangle|^2 = \frac{1}{\pi^2 k_i^2 k_f^2} \sum_{l=0}^{\infty} (2l+1) J_l, \quad (24)$$

where we denote

$$J_l = \left| \int_0^{\infty} dr \psi_{l, \mathbf{k}_f}^{-*}(r) \psi_{l, \mathbf{k}_i}^{+}(r) \right|^2. \quad (25)$$

The total cross section becomes

$$\sigma = \frac{32\pi}{E_i^{3/2} E_f^{1/2}} \frac{1}{R^2} \frac{a_A^3 a_D^3}{(a_A^2 + a_D^2)^3} \exp\left(-\frac{R^2}{a_A^2 + a_D^2}\right) \sum_{l=0}^{\infty} (2l+1) J_l. \quad (26)$$

The  $J_l$  is the square of the overlap of the radial wave functions describing the incoming and outgoing electrons, which correspond to different potentials. The larger the  $l$ , the more the radial wave functions are pushed out of the vicinity of the system's center of mass by the angular momentum barrier. It is only in the vicinity of the center where the two potentials differ. When the classical turning points, solutions  $r$  of the equation

$$\frac{l(l+1)}{r^2} = k^2, \quad (27)$$

for the two wave functions, are outside the region where the potentials differ, they correspond to approximately identical potentials, and their overlap approaches  $\sim \delta(\mathbf{k}_i - \mathbf{k}_f)$ . If we assume that the energies of the acceptor spin-orbital of A and the donor spin-orbital of D are different (which is the case if  $A \neq D^+$ ), the overlap approaches zero. This discussion can be summarized by the claim that as  $l(l+1)/K_{AV}^2$  increases with  $l$ ,  $J_l$  decreases. For the value of  $K_{AV}^2$ , we use

$$K_{AV}^2 = (a_A + R)^2 E_i + (a_D + R)^2 E_f, \quad (28)$$

the average of  $r^2 k^2$  of the in- and out-channels, where  $r$  is the extent of the radial potential approximated by  $R$  plus the acceptor/donor

orbital width and  $k$  is the corresponding wave number. In our model, we assume an exponential decrease of  $J_l$ ,

$$J_l \approx C \exp\left(-\frac{l(l+1)}{K_{AV}^2}\right). \quad (29)$$

Let us summarize the results. Within our model, the total ICEC cross section is given by the sum of two contributions,

$$\sigma_{\text{model}} = \sigma_{\text{VPA}} + \sigma_{\text{ETM}}, \quad (30)$$

where the first term is given by the VPA (4) and the latter term is the electron transfer contribution in a simplified model (26), with  $J_l$  being given by (29) and  $K_{AV}^2$  being given by (28). We call the second contribution the electron transfer model (ETM). In principle, we should add the two contributions coherently, at the level of the scattering amplitudes (3). However, our incoherent sum should differ only for  $R$ , where the absolute values of the two contributions are comparable. The VPA and ETM cross sections depend on  $R$  as  $R^{-6}$  and  $R^{-2} \exp(-\beta R^2)$ , respectively; therefore, they should be comparable only in a limited interval of  $R$ . Thanks to this, the incoherent sum should suffice. The model contains three parameters:  $a_A$ ,  $a_D$ , and  $C$ . Our goal is to either relate these to the tabulated parameters of the subsystems or give their universal values so that we can use the model to estimate the ICEC cross sections in various systems without performing any *ab initio* calculations.

### III. THE R-MATRIX METHOD

#### A. Theory

We use the R-matrix method<sup>10</sup> to calculate the *ab initio* cross sections of the ICEC process. More specifically, we utilize its implementation in the UKRmol+ suite.<sup>11</sup>

In the R-matrix method, we divide the configuration space into two regions separated by the so-called R-matrix sphere of radius  $a$ . In the inner region, the  $(N+1)$ -electron eigenstates are found in the form of the close-coupling expansion,

$$\begin{aligned} \Psi_k^{N+1} = & \hat{A} \sum_{ij} c_{ijk} \Phi_i^N(\mathbf{x}_1, \dots, \mathbf{x}_N) \eta_{ij}(\mathbf{x}_{N+1}) \\ & + \sum_m b_{mk} \chi_m^{N+1}(\mathbf{x}_1, \dots, \mathbf{x}_{N+1}). \end{aligned} \quad (31)$$

The first term is a sum of antisymmetrized products of an  $N$ -electron target state  $\Phi_i^N$  and a continuum spin-orbital  $\eta_{ij}$ . The second term contains the so-called  $L^2$  configurations where all  $N+1$  electrons are bound in the target system. The  $\mathbf{x}$  coordinates comprise the spatial coordinates  $\mathbf{r}$  and the spin index  $\xi$ . The coefficients  $c_{ijk}$  and  $b_{mk}$  are obtained from the diagonalization

$$(\hat{H} + \hat{L}) \Psi_k^{N+1} = E_k \Psi_k^{N+1}, \quad (32)$$

where  $\hat{H}$  is the  $(N+1)$ -electron Hamiltonian and  $\hat{L}$  is the Bloch operator ensuring the hermiticity of the diagonalized operator.

The R-matrix is constructed from these states' surface amplitudes and energies on the R-matrix sphere. The exchange and correlation between the continuum electron and the target are neglected in the outer region. Here, the interaction is treated on the level of the

**TABLE I.** Computational details of the R-matrix calculations for the systems studied. The three numbers given in the *orbitals* column are the number of core/active/virtual orbitals used. They were chosen from the set of molecular orbitals in energy order. The column *states* specifies the number of target states used in the scattering calculations. BTO/GTO specifies the type of continuum basis functions used. For both types, the first number specifies the highest partial wave included. For BTOs, the next two numbers give the number of the radial B-splines and their order. The GTOs used were taken from the continuum basis sets included in the UKRmol+*scripts*<sup>15</sup> release.

System	Basis	Orbitals	States	$a$	$r_{\text{af}}$	Continuum
(HeNe) <sup>+</sup>	cc-pVDZ	2/8/4	20	13	80	GTO, 6
$C_{\infty v}$ , (HeH <sub>2</sub> ) <sup>+</sup>	cc-pVTZ	0/7/4	20	13	80	GTO, 6
(ArHe) <sup>+</sup>	cc-pVDZ	6/4/0	4	17	80	BTO, 6, 30, 8
(LiNa) <sup>+</sup>	cc-pVDZ	6/2/0	2	51	120	BTO, 6, 30, 8
(LiNe) <sup>+</sup>	cc-pVDZ	3/4/0	14	30	120	BTO, 4, 30, 8
(HeNa) <sup>+</sup>	cc-pVDZ	5/2/0	4	26	120	BTO, 6, 30, 8
$C_{2v}$ , (HeH <sub>2</sub> ) <sup>+</sup>	cc-pVTZ	0/7/4	20	13	80	GTO, 6
$C_{\infty v}$ , (ArH <sub>2</sub> ) <sup>+</sup>	cc-pVDZ	6/4/0	4	20	80	BTO, 4, 20, 9

first few terms of the multipole expansion of the Coulomb interaction between the continuum electron and the charge density of the target. The time-independent Schrödinger equation for the continuum electron is translated into an equation for the R-matrix. Using this equation, we propagate the R-matrix from the R-matrix sphere outward to a sphere of radius  $r_{\text{af}}$ . At this outer sphere, we use the R-matrix to match the radial wave functions from the inner region to their asymptotic form, obtaining the scattering matrices and, from them, the sought-after cross sections.

#### B. Computational details

We studied eight different systems. The system-specific computational details are gathered in Table I. We used MOLPRO<sup>12-14</sup> to optimize the molecular orbitals for the (positively charged) target or the neutral target (target + one additional electron) using the Hartree-Fock method. The optimization for the neutral target was used only for (ArH<sub>2</sub>)<sup>+</sup>, because for this system, it better reproduced the asymptotic threshold energies. The scattering models were built from configurations

$$(\text{core} + \text{active})^N (\text{continuum})^1, \quad (33)$$

$$(\text{core} + \text{active})^{N+1}, \quad (34)$$

$$(\text{core} + \text{active})^N (\text{virtual})^1, \quad (35)$$

where the target molecular orbitals are divided into four groups: the *core* orbitals are doubly occupied in all  $N$  and  $(N+1)$  electron states, the *active* orbitals are used as an active space in the  $N$ -electron state calculation, the *virtual* orbitals are only used in the  $(N+1)$ -electron configurations, and the remaining orbitals are discarded. For all systems, the multipole expansion of the potential in the outer region was retained up to second order.

### IV. RESULTS AND DISCUSSION

The first five systems studied (above the horizontal line in Table I) are used to finalize the definition of the model, i.e., to specify how to obtain the parameters  $a_A$ ,  $a_D$ , and  $C$  from the properties



of the two species. The model is then benchmarked by comparing the R-matrix cross sections with the VPA and the model estimates at a distance  $R$  comparable to the size of the system. For benchmarking, we use all eight systems from Table I and, additionally, the ICEC cross sections in  $(\text{H}_2\text{O} + \text{H})^+$  studied in Ref. 16. The asymptotic thresholds of the considered processes can be found in the Appendix.

### A. Setting up the model

We performed the R-matrix calculations of ICEC cross sections for the following systems:  $(\text{HeNe})^+$ ,  $(\text{ArHe})^+$ ,  $(\text{LiNe})^+$ ,  $(\text{LiNa})^+$ , and  $(\text{HeH}_2)^+$  for a  $C_{\infty v}$  geometry, i.e., all three nuclei are in one line. Calculations were run for a series of distances  $R$  between the centers of mass of the two subsystems, and both ICEC processes were considered for each system [e.g., the processes  $\text{He} + \text{Ne}^+ \rightarrow \text{He}^+ + \text{Ne}$  and  $\text{He}^+ + \text{Ne} \rightarrow \text{He} + \text{Ne}^+$  for the system  $(\text{HeNe})^+$ ]. Then, we have fitted the R-matrix cross sections to the sum (30) of the VPA (4) and ETM (26) expressions with respect to  $R$  and  $E_i$  with the fitting parameters being  $a_A$ ,  $a_D$ , and  $C$ . The photoionization cross sections were taken from Ref. 17 for the noble gases, from Ref. 18 for  $\text{H}_2$ , and from TOPbase<sup>19</sup> for the alkali metals.

In Fig. 1, we compare the R-matrix, VPA, ETM, and VPA + ETM cross sections, where the ETM parameters have been specified by fitting VPA + ETM to the R-matrix results, for two possible ICEC processes in  $(\text{HeNe})^+$ . For  $R \geq 8$  a.u., the asymptotic VPA (4) is in agreement with the R-matrix cross sections. For all smaller  $R$ , the ETM gives a better estimation of the *ab initio* data than the VPA. By comparing the two contributions to the total fitted cross sections (the dashed and dotted lines), we see that they have equal magnitudes for  $\approx 7.3$  a.u. and are comparable in an interval of width  $\lesssim 1$  a.u. around this value. In this region, it would be more accurate to add the two contributions coherently, but the relative size of the relevant interval with respect to the whole investigated interval justifies the usage of the incoherent sum. The equilibrium distance in the  $\text{HeNe}^+$  dimer averaged over the asymptotically degenerate ground states is  $\approx 4$  a.u.,<sup>20</sup> where the VPA underestimates the cross section by more than two orders of magnitude. For this interatomic distance, the fitted ETM slightly overestimates it but is far more accurate than the VPA.

The  $a_A$  and  $a_D$  parameters of the model are the widths of the Gaussians used to approximate the acceptor/donor orbitals. These widths are related to the radii of the corresponding atoms. In our model, we want to estimate the  $a$  parameters as

$$a = \alpha r, \quad (36)$$

where  $r$  is a well-defined and tabulated atomic radius and  $\alpha$  is a constant universal for all the systems. We correlate the fitted parameters with the covalent<sup>21</sup> and the van der Waals radii,<sup>22</sup> see Fig. 2. We are correlating a sum of squares of the fitted parameters for each process rather than the  $a$  parameters themselves. This is because  $a_A$  and  $a_D$  in formula (26) are not independent. We have, therefore, fitted the combination mentioned above to ensure better convergence of the fit and smaller resulting standard deviations.

This figure suggests that the covalent radius works better than the van der Waals radius at being proportional to the width parameters of the used Gaussians. The linear fit results of both types of

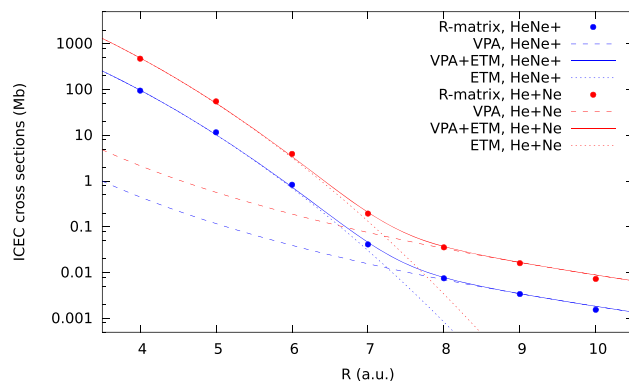


**FIG. 1.** ICEC cross sections for  $\text{He} + \text{Ne}^+ \rightarrow \text{He}^+ + \text{Ne}$  (blue) and  $\text{He}^+ + \text{Ne} \rightarrow \text{He} + \text{Ne}^+$  (red). Dots are the *ab initio* R-matrix results, the dashed line is the VPA contribution (4), the solid line is the VPA + ETM contribution, and the dotted line is the ETM contribution (26). The parameters of ETM were determined by fitting the VPA + ETM to the R-matrix cross sections. For both processes,  $E_{\text{vph}} = 29.56$  eV, which for the first process means  $E_i = 8.00$  eV and  $E_f = 4.97$  eV and vice versa for the reverse process.

atomic radii are in Table II. The rms of residuals also speaks in favor of the covalent radius.

We analyzed the fitted values of  $C$  for the processes with respect to the physical parameters of the respective particles. Based on this, we impose an ad hoc dependence on the difference of the energies of the incoming electron and the outgoing electron in the following form:

$$C = \bar{C} \exp\left(-\frac{|E_{A_A} - I_{P_D}|}{d}\right), \quad (37)$$

where  $\bar{C}$  and  $d$  are fitting parameters. The  $C$  values for all the processes and the fit to function (37) are shown in Fig. 3. The resulting values of the fitting parameters are given in Table II.

The parameters of the ETM (26), (28), and (29) are now determined. The value of  $C$  is given via (37), where the values of  $\bar{C}$  and  $d$  are given in Table II. The parameters  $a_A$  and  $a_D$  are proportional to the covalent radius of the given atom, Eq. (36), where the value of the constant of proportionality  $\alpha$  is specified in Table II. For  $\text{H}_2$ , the effective radius is given as the sum of the covalent radius of H and the half of the  $\text{H}_2$  bond length. We estimate the ICEC cross sections with the sum (30) of the VPA (4) and ETM contributions.

### B. Benchmarking the model

Now, we want to compare the cross sections estimated by the model with the *ab initio* ones. We compare the values for three other systems in addition to the systems used for fitting the model's parameters. These are  $(\text{HeNa})^+$ ,  $(\text{HeH}_2)^+$  for a  $C_{2v}$  geometry, and  $(\text{ArH}_2)^+$  for a  $C_{\infty v}$  geometry.

The results for  $(\text{HeH}_2)^+$  are shown in Fig. 4 in comparison with the VPA and VPA + ETM. In this case, the R-matrix cross sections do not converge to the asymptotics given by the VPA formula; instead, they behave as approximately twice the VPA formula (the dotted line). The reason could be that for molecules, the VPA formula in Eq. (4) describes the cross sections averaged over the orientations of the two particles, but here we have results for one fixed

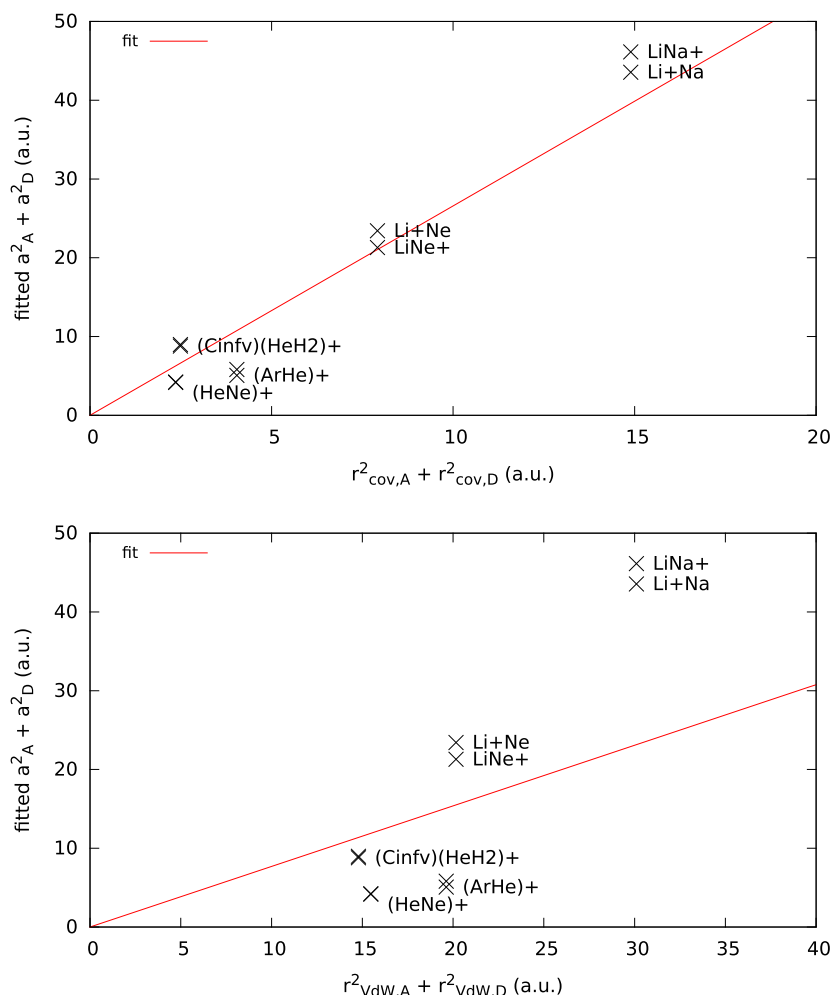


**FIG. 2.** Correlation of the fitted  $a_A^2 + a_D^2$  with  $r_{x,A}^2 + r_{x,D}^2$ , where  $x$  stands for the covalent radius (top panel) or the van der Waals radius (bottom panel). The red line is a linear fit. For  $H_2$ , the hydrogen atomic radius plus half of the  $H_2$  bond length was used as the  $H_2$  effective radius. In both graphs, the crosses for  $(HeH_2)^+$  (in  $C_{\infty v}$ ) and  $(HeNe)^+$  are doubled because the fitted parameters obtained from both directions of ICEC coincide.

**TABLE II.** Above the horizontal line: Results of the linear fit of  $a = \alpha r_x$  of the data shown in Fig. 2. Below the horizontal line: Results of the fit of function (37) to the data shown in Fig. 3.

Parameter	Value	Std. error	rms of res.
$\alpha$ (for $r_{cov}$ )	1.63	0.07	0.57
$\alpha$ (for $r_{vdW}$ )	0.88	0.10	1.39
$\bar{C}$	9	5	1.20
$d$	1.9 eV	0.3 eV	

orientation of  $H_2$ . Another possibility is that the target model is not accurate enough or that the partial waves of the continuum electron, not included in the calculation, contribute. Considering the rescaled VPA, the R-matrix converges to this asymptote at  $R = 11$  a.u. The VPA + ETM cross sections give better estimates for  $R \lesssim 8$  a.u. The equilibrium distance of the  $HeH_2^+$  dimer in the  $C_{2v}$  orientation is

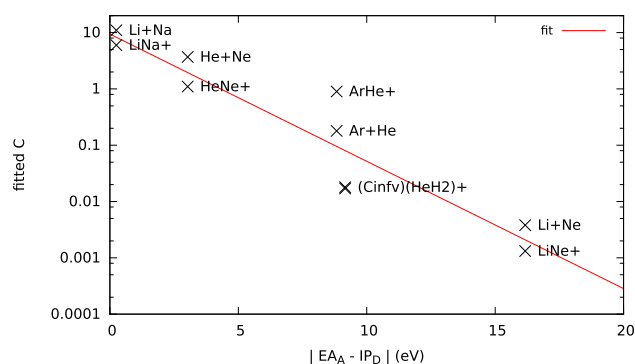


**FIG. 3.** Dependence of the fitted  $C$  parameters on the absolute value of the difference of the energy of the electron affinity of the acceptor and the ionization energy of the donor. The red line is a fit of function (37). There is a double cross for  $(HeH_2)^+$  (in  $C_{\infty v}$ ) because the fitted  $C$  values obtained from both directions of ICEC coincide.

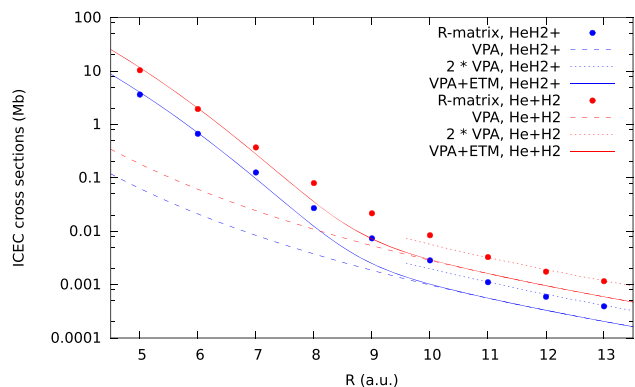


**FIG. 4.** ICEC cross sections for  $\text{He} + \text{H}_2^+ \rightarrow \text{He}^+ + \text{H}_2$  (blue) and  $\text{He}^+ + \text{H}_2 \rightarrow \text{He} + \text{H}_2^+$  (red). The nuclei are in a  $C_{2v}$  geometry, i.e., the line connecting the two H nuclei is perpendicular to the line connecting the He nucleus and the center of mass of  $\text{H}_2$ . Dots are the *ab initio* R-matrix results, the dashed line is the VPA, the solid line is the model VPA + ETM, and the dotted line is the VPA multiplied by 2. For both processes,  $E_{\text{vph}} = 27.43$  eV, which for the first process means  $E_i = 12.00$  eV and  $E_f = 3.84$  eV and vice versa for the reverse process.

$\approx 4.5$  a.u.<sup>23</sup> At  $R = 5$  a.u., the VPA underestimates the R-matrix by almost two orders of magnitude, and the model is far more accurate.

In Table III, we can see the comparisons of the cross sections obtained from the R-matrix, the VPA, and the model for one value

of  $R$  and  $E$  for each process. The  $R$  value was chosen among the ones used for R-matrix calculations such that the energy of the ground state of the target is minimal. The energy was selected so that the R-matrix cross sections are reliable in the sense that the continuum basis provides a good description and other ICEC channels (that we have not included in the calculations) are closed. We compare the logarithmic error (see Table III).

For all already mentioned processes, both included and excluded from the fitting, the model estimates the R-matrix values better than the VPA. For the chosen interparticle distances, it is, on average, two orders of magnitude closer. For all systems, except  $(\text{HeNa})^+$ , the model prediction is within one order of magnitude from the *ab initio* cross section.

Apart from all the models we have considered so far, we have also compared the R-matrix, VPA, and the model for ICEC in  $(\text{H} + \text{H}_2\text{O})^+$ . The computational details and full analysis of the R-matrix results can be found in Ref. 16. Let us only summarize relevant information. In all calculations, the H atom was on the  $C_2$  axis of the  $\text{H}_2\text{O}$  molecule. In  $\text{H}-\text{H}_2\text{O}$ , the H was on the H side of the  $\text{H}_2\text{O}$  molecule, and in  $\text{H}_2\text{O}-\text{H}$ , it was on the O side of the  $\text{H}_2\text{O}$  molecule. When the initial state is  $\text{H}^+ + \text{H}_2\text{O}$ , the process is denoted P, and when it is  $\text{H} + \text{H}_2\text{O}^+$ , it is denoted W.

In our model, we used the covalent radius of hydrogen plus half of the OH bond for the effective radius and included the first excited state of  $\text{H}_2\text{O}^+$  as the only state produced by the ICEC process, motivated by the discussion in Ref. 16. For  $\text{H}_2\text{O}-\text{H}$  ICEC-W,

**TABLE III.** Comparison of the *ab initio* R-matrix cross sections with the predictions of the VPA and the model (VPA + ETM) for one value of  $R$  and  $E$  for each process. The last two columns compare the logarithmic errors of the two approximations. The processes above the upper horizontal line have been used to fit the model, as opposed to the ones below. The R-matrix cross sections below the lower horizontal line were taken from Ref. 16; see the text for details.

Process	$R$ (a.u.)	$E$ (eV)	Cross sections (Mb)			$\log\left(\frac{\text{VPA}}{\text{R-matrix}}\right)$	$\log\left(\frac{\text{model}}{\text{R-matrix}}\right)$
			R-matrix	VPA	Model		
$\text{HeNe}^+ \rightarrow \text{He}^+\text{Ne}$	4.0	5.00	$1.54 \times 10^2$	$1.02 \times 10^0$	$1.11 \times 10^3$	-2.18	0.86
$\text{He}^+\text{Ne} \rightarrow \text{HeNe}^+$	4.0	5.00	$1.29 \times 10^3$	$7.80 \times 10^0$	$2.81 \times 10^3$	-2.22	0.34
$\text{ArHe}^+ \rightarrow \text{Ar}^+\text{He}$	5.0	13.00	$7.35 \times 10^1$	$2.19 \times 10^0$	$5.10 \times 10^1$	-1.53	-0.16
$\text{Ar}^+\text{He} \rightarrow \text{ArHe}^+$	5.0	13.00	$2.35 \times 10^0$	$2.34 \times 10^{-1}$	$1.59 \times 10^1$	-1.00	0.83
$\text{LiNe}^+ \rightarrow \text{Li}^+\text{Ne}$	4.0	21.10	$7.73 \times 10^0$	$7.06 \times 10^{-2}$	$8.30 \times 10^0$	-2.04	0.03
$\text{Li}^+\text{Ne} \rightarrow \text{LiNe}^+$	4.0	21.10	$2.73 \times 10^0$	$1.98 \times 10^{-1}$	$2.12 \times 10^0$	-1.14	-0.11
$\text{LiNa}^+ \rightarrow \text{Li}^+\text{Na}$	10.0	2.00	$7.99 \times 10^3$	$1.24 \times 10^{-3}$	$1.24 \times 10^4$	-6.81	0.19
$\text{Li}^+\text{Na} \rightarrow \text{LiNa}^+$	10.0	2.00	$1.83 \times 10^4$	$1.41 \times 10^{-3}$	$1.41 \times 10^4$	-7.11	-0.11
$C_{\infty v}, \text{HeH}_2^+ \rightarrow \text{He}^+\text{H}_2$	5.0	11.00	$5.44 \times 10^0$	$1.69 \times 10^{-1}$	$6.60 \times 10^0$	-1.51	0.08
$C_{\infty v}, \text{He}^+\text{H}_2 \rightarrow \text{HeH}_2^+$	5.0	11.00	$3.37 \times 10^1$	$1.01 \times 10^0$	$3.95 \times 10^1$	-1.52	0.07
$\text{HeNa}^+ \rightarrow \text{He}^+\text{Na}$	5.0	22.50	$2.30 \times 10^0$	$5.81 \times 10^{-3}$	$9.54 \times 10^{-2}$	-2.60	-1.38
$\text{He}^+\text{Na} \rightarrow \text{HeNa}^+$	5.0	22.50	$1.77 \times 10^1$	$1.07 \times 10^{-2}$	$6.72 \times 10^{-1}$	-3.22	-1.42
$C_{2v}, \text{HeH}_2^+ \rightarrow \text{He}^+\text{H}_2$	5.0	14.00	$3.63 \times 10^0$	$6.31 \times 10^{-2}$	$4.00 \times 10^0$	-1.76	0.04
$C_{2v}, \text{He}^+\text{H}_2 \rightarrow \text{HeH}_2^+$	5.0	14.00	$1.03 \times 10^1$	$1.83 \times 10^{-1}$	$1.59 \times 10^1$	-1.75	0.19
$C_{\infty v}, \text{ArH}_2^+ \rightarrow \text{Ar}^+\text{H}_2$	6.0	2.00	$9.85 \times 10^3$	$9.86 \times 10^0$	$8.81 \times 10^3$	-3.00	-0.05
$C_{\infty v}, \text{Ar}^+\text{H}_2 \rightarrow \text{ArH}_2^+$	6.0	2.00	$2.06 \times 10^3$	$3.94 \times 10^0$	$1.05 \times 10^4$	-2.72	0.71
$\text{H}-\text{H}_2\text{O}$ ICEC-P	5.5	3.30	$5.25 \times 10^3$	$6.87 \times 10^0$	$3.39 \times 10^2$	-2.88	-1.19
$\text{H}-\text{H}_2\text{O}$ ICEC-W	5.5	3.82	$3.97 \times 10^1$	$1.11 \times 10^0$	$1.86 \times 10^2$	-1.55	0.67
$\text{H}_2\text{O}-\text{H}$ ICEC-P	5.8	4.02	$1.54 \times 10^3$	$3.86 \times 10^0$	$1.66 \times 10^2$	-2.60	-0.97
$\text{H}_2\text{O}-\text{H}$ ICEC-W	5.8	4.28	$7.51 \times 10^0$	$7.03 \times 10^{-1}$	$1.10 \times 10^2$	-1.03	1.17



the model overestimates the cross sections such that it is a similarly good estimate as the VPA. In this system, the electron transfer contributions to the cross sections for ICEC-P and ICEC-W differ by more than two orders of magnitude. In our model, the only asymmetry is introduced by the energies  $E_i$  and  $E_f$ , which at the same continuum energy switch values for ICEC-P and ICEC-W. The difference of these values is given by the difference of the ionization energies of the states active in ICEC. In the  $(\text{H} + \text{H}_2\text{O})^+$  system, this is not enough to describe the asymmetry of the two processes. This is the reason for the noticeable underestimation of ICEC-P and overestimation of ICEC-W by the model. Nevertheless, only for the  $\text{H}_2\text{O}-\text{H}$  ICEC-W process, we obtain an estimate similarly precise as the VPA, whereas, in the other three processes, the model is approximately an order of magnitude closer to the R-matrix cross sections.

## V. CONCLUSION

We have developed an analytical model that predicts the interatomic Coulombic electron capture cross sections beyond the virtual photon approximation. While the new model is more accurate than the virtual photon at distances where the two involved species interact, it keeps a simple description of the whole system as two independent entities. Furthermore, using R-matrix calculations, we have demonstrated that the parameters of our novel formula can be taken from the properties of each species. Our model reduces the error by about two orders of magnitude on average with respect to the virtual photon approximation at interatomic distances comparable to the size of the involved species when tested against R-matrix ICEC cross sections.

## ACKNOWLEDGMENTS

N.S. and J.Š. acknowledge the ANR-DFG for the financial support of the QD4ICEC project (Grant No. ANR-22-CE92-0071-01) and the Indo-French Centre for the Promotion of Advanced Research—CEFIPRA (Project No. 6704-2). V.G. acknowledges the support from the EPSRC Doctoral Training Partnership under Grant No. EP/T518165/1.

## AUTHOR DECLARATIONS

### Conflict of Interest

The authors have no conflicts to disclose.

## Author Contributions

**Jan Šenk:** Conceptualization (equal); Formal analysis (equal); Investigation (equal); Methodology (equal); Writing – original draft (equal); Writing – review & editing (equal). **Vincent Graves:** Validation (equal); Writing – original draft (equal); Writing – review & editing (equal). **Jimena D. Gorfinkiel:** Validation (equal); Writing – original draft (equal); Writing – review & editing (equal). **Přemysl Koloreň:** Conceptualization (equal); Supervision (equal); Writing – original draft (equal); Writing – review & editing (equal). **Nicolas Sisourat:** Conceptualization (equal); Funding

TABLE IV. Asymptotic thresholds for the ICEC processes.

Process	Threshold (eV)
$\text{HeNe}^+ \rightarrow \text{He}^+\text{Ne}$	3.03
$\text{Ar}^+\text{He} \rightarrow \text{ArHe}^+$	8.83
$\text{Li}^+\text{Ne} \rightarrow \text{LiNe}^+$	16.17
$\text{LiNa}^+ \rightarrow \text{Li}^+\text{Na}$	0.25
$\text{HeH}_2^+ \rightarrow \text{He}^+\text{H}_2$	9.16
$\text{HeNa}^+ \rightarrow \text{He}^+\text{Na}$	19.45
$\text{ArH}_2^+ \rightarrow \text{Ar}^+\text{H}_2$	0.33
ICEC-W	1.06

acquisition (lead); Methodology (equal); Supervision (equal); Validation (equal); Writing – original draft (equal); Writing – review & editing (equal).

## DATA AVAILABILITY

The data that support the findings of this study are available from the corresponding author upon reasonable request.

## APPENDIX: THE ASYMPTOTIC THRESHOLDS FOR THE ICEC PROCESSES

In Table IV, we gather the asymptotic ( $R \rightarrow \infty$ ) thresholds, i.e., the minimal energy of the incoming electron  $E_i$  required for the process to be energetically allowed. The thresholds were evaluated using the conservation of energy (5) and the conditions  $E_i \geq 0$  and  $E_f \geq 0$ . In this table, we can find the thresholds for one ICEC process for each system considered. The reverse of each process in this table has a threshold of 0 eV. The ionization potentials necessary to evaluate the thresholds were taken from Refs. 24 and 25.

## REFERENCES

- 1 K. Gokhberg and L. S. Cederbaum, *J. Phys. B: At., Mol. Opt. Phys.* **42**, 231001 (2009).
- 2 K. Gokhberg and L. S. Cederbaum, *Phys. Rev. A* **82**, 052707 (2010).
- 3 N. Sisourat, T. Miteva, J. D. Gorfinkiel, K. Gokhberg, and L. S. Cederbaum, *Phys. Rev. A* **98**, 020701 (2018).
- 4 A. Molle, A. Dubois, J. D. Gorfinkiel, L. S. Cederbaum, and N. Sisourat, *Phys. Rev. A* **104**, 022818 (2021).
- 5 A. Bande, E. Fasshauer, A. Molle, D. Peláez, F. M. Pont, and N. Sisourat, *J. Phys. B: At., Mol. Opt. Phys.* **56**, 232001 (2023).
- 6 J. R. Taylor, *Scattering Theory: The Quantum Theory on Nonrelativistic Collisions* (Wiley, New York, 1972).
- 7 D. L. Andrews, *Chem. Phys.* **135**, 195 (1989).
- 8 D. P. Craig and T. Thirunamachandran, *Chem. Phys.* **167**, 229 (1992).
- 9 R. Santra and L. S. Cederbaum, *Phys. Rep.* **368**, 1 (2002).
- 10 J. Tennyson, *Phys. Rep.* **491**, 29 (2010).
- 11 Z. Mašín, J. Benda, J. D. Gorfinkiel, A. G. Harvey, and J. Tennyson, *Comput. Phys. Commun.* **249**, 107092 (2020).
- 12 H.-J. Werner, P. J. Knowles, G. Knizia, F. R. Manby, and M. Schütz, *Wiley Interdiscip. Rev.: Comput. Mol. Sci.* **2**, 242 (2012).
- 13 H.-J. Werner, P. J. Knowles, F. R. Manby, J. A. Black, K. Doll, A. Heßelmann, D. Kats, A. Köhn, T. Korona, D. A. Kreplin, Q. Ma, T. F. Miller III,

- A. Mitrushchenkov, K. A. Peterson, I. Polyak, G. Rauhut, and M. Sibaev, *J. Chem. Phys.* **152**, 144107 (2020).
- <sup>14</sup>H.-J. Werner, P. J. Knowles, P. Celani, W. Györfy, A. Hesselmann, D. Kats, G. Knizia, A. Köhn, T. Korona, D. Kreplin, R. Lindh, Q. Ma, F. R. Manby, A. Mitrushchenkov, G. Rauhut, M. Schütz, K. R. Shamasundar, T. B. Adler, R. D. Amos, S. J. Bennie, A. Bernhardsson, A. Berning, J. A. Black, P. J. Bygrave, R. Cimiraglia, D. L. Cooper, D. Coughtrie, M. J. O. Deegan, A. J. Dobbyn, K. Doll, M. Dornbach, F. Eckert, S. Erfort, E. Goll, C. Hampel, G. Hetzer, J. G. Hill, M. Hodges, T. Hrenar, G. Jansen, C. Köppl, C. Kollmar, S. J. R. Lee, Y. Liu, A. W. Lloyd, R. A. Mata, A. J. May, B. Mussard, S. J. McNicholas, W. Meyer, T. F. Miller III, M. E. Mura, A. Nicklass, D. P. O'Neill, P. Palmieri, D. Peng, K. A. Peterson, K. Pflüger, R. Pitzer, I. Polyak, M. Reiher, J. O. Richardson, J. B. Robinson, B. Schröder, M. Schwilk, T. Shiozaki, M. Sibaev, H. Stoll, A. J. Stone, R. Tarroni, T. Thorsteinsson, J. Toulouse, M. Wang, M. Welborn, and B. Ziegler, MOLPRO, version 2012.1, a package of *ab initio* programs.
- <sup>15</sup>K. Houfek, J. Benda, Z. Mašín, A. Harvey, T. Meltzer, V. Graves, and J. D. Gorfinkiel, *Comput. Phys. Commun.* **298**, 109113 (2024).
- <sup>16</sup>V. Graves, J. Šenk, P. Kolorenč, N. Sisourat, and J. D. Gorfinkiel, *J. Chem. Phys.* **160**, 204306 (2024).
- <sup>17</sup>G. V. Marr and J. B. West, *At. Data Nucl. Data Tables* **18**, 497 (1976).
- <sup>18</sup>M. R. Flannery, H. Tai, and D. L. Albritton, *At. Data Nucl. Data Tables* **20**, 563 (1977).
- <sup>19</sup>C. Mendoza, *Phys. Scr.* **1996**, 198.
- <sup>20</sup>J. Seong, K. C. Janda, M. P. McGrath, and N. Halberstadt, *Chem. Phys. Lett.* **314**, 501 (1999).
- <sup>21</sup>P. Pyykkö and M. Atsumi, *Chem. Eur. J.* **15**, 186 (2009).
- <sup>22</sup>M. Mantina, A. C. Chamberlin, R. Valero, C. J. Cramer, and D. G. Truhlar, *J. Phys. Chem. A* **113**, 5806 (2009).
- <sup>23</sup>M. F. Falcetta and P. E. Siska, *Chem. Phys. Lett.* **213**, 531 (1993).
- <sup>24</sup>J. E. Sansonetti and W. C. Martin, "Handbook of basic atomic spectroscopic data," *J. Phys. Chem. Ref. Data* **34**, 1559 (2005).
- <sup>25</sup>*NIST Chemistry WebBook, NIST Standard Reference Database Number 69*, edited by P. J. Linstrom and W. G. Mallard (National Institute of Standards and Technology, Gaithersburg, MD, 2024).